CHEMISTRY
A EUROPEAN JOURNAL

DOI: 10.1002/chem.200801684

Self-Organization, Optical, and Electrical Properties of α-Quinquethiophene–Dinucleotide Conjugates

Silvia Alesi,[a] Giorgia Brancolini,[a] Ilenia Viola,[b] Massimo Luigi Capobianco,[a] Alessandro Venturini,[a] Nadia Camaioni,[a] Giuseppe Gigli,[b] Manuela Melucci,[a] and Giovanna Barbarella*[a]

Abstract: The synthesis and properties of $^{5'}$TA$^{3'}$-t5 (**8a**) and $^{5'}$CG$^{3'}$-t5 (**8b**) conjugates, in which the self-complementary dinucleotides TA and CG are covalently bound to the central ring of α-quinquethiophene (t5), are described. According to molecular mechanics calculations, the preferred conformation of both **8a** and **8b** is that with the dinucleotide folded over the planar t5 backbone, with the nucleobases facing t5 at stacking distance. The calculations show that the aggregation process of **8a** and **8b** is driven by a mix of nucleobase-thiophene interactions, hydrogen bonding between nucleobases (*non* Watson–Crick (W&C) in TA, and W&C in CG), van der Waals, and electrostatic interactions. While **8b** is scarcely soluble in any solvents, **8a** is soluble in water, indicating that the aggregates of the former are more stable than those of the latter. Microfluidic-induced self-assembly studies of **8a** showed the formation of lamellar, spherulitic, and dendritic supramolecular structures, depending on the concentration and solvent evaporation time. The self-assembled structures displayed micrometer dimensions in the *xy* plane of the substrate and nanometer dimensions in the *z* direction. Spatially resolved confocal microscopy and spectroscopy showed that the aggregates were characterized by intense fluorescence emission. Cast films of **8a** from water solutions showed chirality transfer from the dinucleotide to t5. The hole mobility of the cast films of **8a** was estimated using a two-electrode device under high vacuum and found to be up to two orders of magnitude greater than those previously measured for dinucleotide–quarterthiophene conjugates under the same experimental conditions.

Keywords: conducting materials · oligonucleotides · photoluminescence · self-assembly · supramolecular chemistry · thiophene

Introduction

One of the most appealing properties of thiophene materials is their "plasticity": the capability to undergo small bond-length and angle deformations extended over the entire aromatic skeleton in order to maximize the intermolecular interactions.[1] The low energy barriers for conformational interchange through inter-ring rotations and the aggregation modalities governed by a plethora of weak and directional interactions (π–π stacking, hydrogen bonding, sulfur–sulfur contacts and so forth[2]) may induce polymorphism[3,1d] and make it difficult to predict the solid-state arrangement and related functional properties merely by inspection of the molecular structure. Finding a way to control the supramolecular organization of functional thiophene oligomers and polymers is challenging, because they are among the best semiconducting and fluorescent conjugated materials, and their performance in devices such as field-effect transistors, light-emitting diodes, or photovoltaic cells is strictly related to the way they self-organize in thin films.[4] Among the various strategies towards this goal, molecular self-assembly directed by appropriate functionalization is a powerful bottom-up method.[5,6] Of all possible functionalization types, the use of biological components like DNA bases or small proteins looks like one of the promising possibilities.[6]

[a] Dr. S. Alesi, Dr. G. Brancolini, Dr. M. L. Capobianco, Dr. A. Venturini, Dr. N. Camaioni, Dr. M. Melucci, Dr. G. Barbarella
Consiglio Nazionale Ricerche
Istituto per la Sintesi Organica e la Fotoreattività (ISOF-CNR)
Via P. Gobetti 101, 40129 Bologna (Italy)
Fax: (+39) 051-6398-349
E-mail: barbarella@isof.cnr.it

[b] Dr. I. Viola, Dr. G. Gigli
National Nanotechnology Laboratory (NNL) of INFM-CNR and Dip. Ingegneria Innovazione, Università del Salento
Via Arnesano, 73100 Lecce (Italy)

Supporting information for this article is available on the WWW under http://dx.doi.org/10.1002/chem.200801684.

The biocomponents being capable of self-assembly through known biorecognition principles, one can expect that it would be possible to program the supramolecular aggregation modalities of the semiconductor moieties simply by choosing the appropriate biocomponents.

So far, only a few papers have been reported describing the fuctionalization of conjugated semiconducting materials with biocomponents.[7] A few studies are focused on the ability of the biocomponents to induce self-assembly into helical structures. Iwaura et al.[7a] reported the synthesis of a thymidine-functionalized oligo(*p*-phenylenevinylene) and examined its self-assembling properties with a complementary polyadenosine strand in aqueous solution, demonstrating that T···A base pairing was able to induce the helical stack of the oligo(*p*-phenylenevinylene) moieties. Bauerle et al.[7b] reported the "click synthesis" of a quaterthiophene functionalized with the self-complementary adenine and thymine nucleosides, and found that thanks to T···A self-recognition the oligomer was able to form fibers up to 30 μm in length on highly oriented pyrolytic graphite after annealing at 120 °C. Nevertheless little is known about the way this type of functionalization affects the optical and electrical properties of the semiconducting moiety. Information on this point would be relevant to another important field of research, namely that concerning the use of charged conjugated polymers as optical and electrical transducers in biosensors for the detection of DNA, proteins or biologically relevant ions.[8] Leclerc et al.[8a] demonstrated that the conformational changes of the aromatic backbone induced by interaction of cationic polythiophenes with single- or double-stranded DNA result in variations of absorption and emission wavelengths that allow the direct detection of single nucleotide polymorphism from clinical samples in only a few minutes. Inganas et al.[8c] demonstrated that the interactions with DNA and the optical phenomena observed in solution persisted when the charged polythiophene was deposited and patterned on a surface, offering a new way to create inexpensive gene chips for the rapid detection of DNA hybridization or the sensing of single-nucleotide polymorphism.

In this framework, we have recently started an investigation aimed at gaining information on the nature of the interactions between thiophene derivatives and DNA components by means of the synthesis of model oligothiophene-oligonucleotide "hybrid" molecules. We intended to explore hybrids of different size and substitution pattern, to study the way they interact and self-organize in solution and in cast films, and how the presence of the biosubstituents affects their optical and electrical properties. We chose to start with α-quaterthiophene and α-quinquethiophene, both non-commercial compounds and among the best organic semiconductors with high charge carrier mobility.[9,10] We have already reported the synthesis of a structurally homogeneous series of quaterthiophene derivatives bearing dinucleotide substitutents at both terminal positions.[7c] We showed that the quaterthiophene–dinucleotide conjugates self-assemble, forming rods of micrometer length, and that fine changes occur in supramolecular organization, photoluminescence, and charge conductivity on changing the dinucleotide scaffold.[7c] In the present paper we describe the synthesis (from compounds **1** and **2** via intermediates **3**–**7**) and the properties of two dinucleotide-functionalized α-quinquethiophenes (**8a**, **8b**) bearing in the central position a self-complementary dinucleotide, TA or CG, capable of Watson–Crick base pairing.

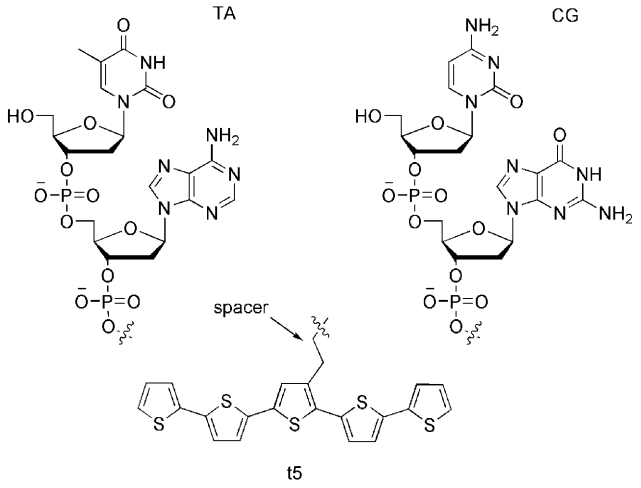

Molecular mechanics and molecular dynamics calculations were carried out to gain insight into the conformational properties and the aggregation mechanisms of these conjugates.

Conjugate **8b** proved to be scarcely soluble in all solvents, including water, and only UV/Vis, CD, and PL spectra in dilute solution could be analyzed. However, compound **8a** was soluble in water at sufficient concentration and could be investigated by means of UV/Vis, CD, and PL spectroscopy in solution and cast film, microfluidic-induced self-assembly, atomic force microscopy, and spatially-resolved confocal microscopy and spectroscopy. Moreover, cast films of **8a** from water were electrically characterized under high vacuum using a two-electrode device.

Results and Discussion

Synthesis: Conjugates **8a** and **8b** were prepared according to the procedures reported in Scheme 1.

Quinquethiophene **3** was obtained in 55% yield by Stille coupling of the 2,5-dibromo-3-thiophene-ethanol (**1**) with 5-tributylstannyl-2,2′-bithiophene (**2**) using [$Pd(Ph_3)_4$] as catalyst. The oligomer **3** was then reacted with an excess of 5′-protected (4,4′-dimethoxytrityl)-deoxy-dinucleotides previously phosphorylated. After removal of the protecting groups, the target compounds **8a** and **8b** were separated from the crude mixture by reversed-phase chromatography.

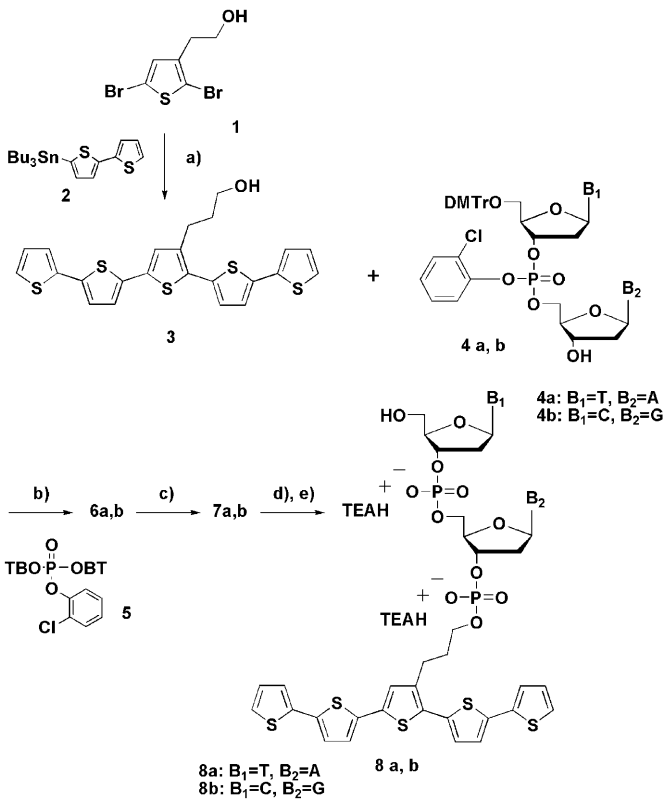

Scheme 1. a) $[PdP(Ph_3)_4]$, toluene, reflux, overnight; b) compound **5**, py, 2 h, RT; c) benzenesulfonic acid, $MeOH/CH_2Cl_2$, 0.5 h, RT; d) py, 16 h, RT; e) NH_3 30%, 24 h, 50°C. DMTr = 4,4′-dimethoxytrityl, BT = benzotriazolyl, TEA = triethylamine.

The detailed synthetic procedures and the mass spectroscopy, ^1H and ^{31}P NMR characterizations are reported as Supporting Information.

Molecular modeling: Computational techniques within the framework of a molecular mechanics approach were used to explore the conformational preferences of the conjugates **8a** and **8b**. For their aggregates, extensive conformational searches were carried out using "simulated annealing" protocols in an iterative fashion within the Amber force field as implemented in the Macromodel program.[11a, b] The calculations were performed with an implicit solvent model, which was used to account for the presence of water, and with reduced charges on the phosphate groups[11c] to simulate the presence of the counterions in solution.[11d] For both 5′TA3′-t5 and 5′CG3′-t5 monomers two principal conformations were found, one with both DNA bases facing the t5 backbone and the other with only one base facing t5 (Figure 1, monomers I and II, respectively). In both systems monomer I is more stable than monomer II, although by only a few $kJ\,mol^{-1}$. As shown in Figure 1, in the case of monomer I of 5′TA3′-t5 the nucleobases form a non-W&C hydrogen-bonded base pair lying parallel to the t5 plane. The energy difference with monomer II is about $8\,kJ\,mol^{-1}$. In the case of monomer I of $^{5'}CG^{3'}$-t5, the nucleobases are not hydrogen bonded and the energy difference with monomer II is only $4\,kJ\,mol^{-1}$. For both compounds the nucleobases are at stacking distance from the planar t5 backbone, indicating that stacking interactions play an important role in the stabilization of the monomers.

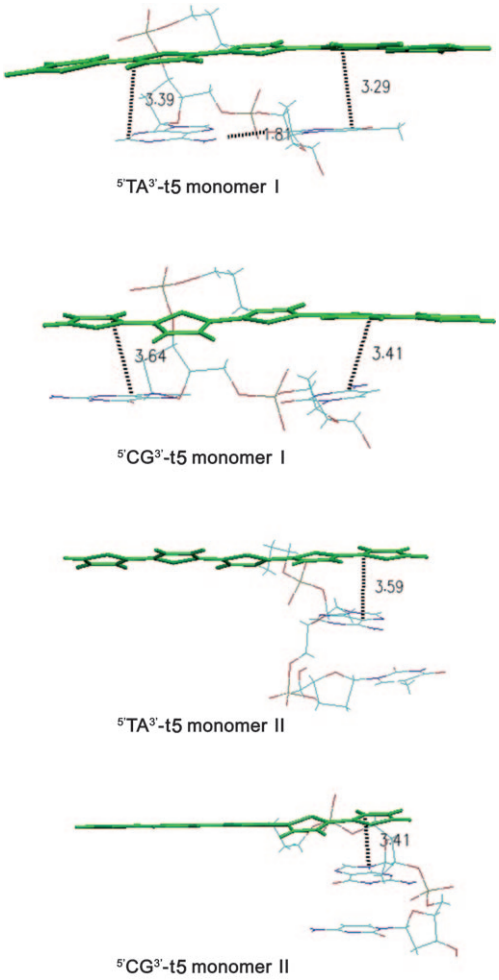

Figure 1. Most stable conformations of conjugates **8a** and **8b** and nucleobase-thiophene stacking distances.

Among all the possible dimers derived from these structures, three (A, B, and C) have been found to be the most stable and are reported in Figures 2 and 3, with the corresponding energies given in Table 1. Monomers I are more stable than monomers II by 8 and $4\,kJ\,mol^{-1}$ for **8a** and **8b**, respectively.

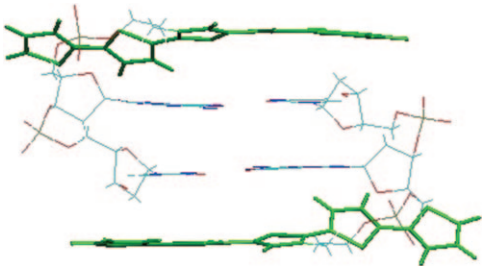

Figure 2. Most stable dimer C of $^{5'}CG^{3'}$-t5 (**8b**) with formation of a W&C helix between the nucleobases.

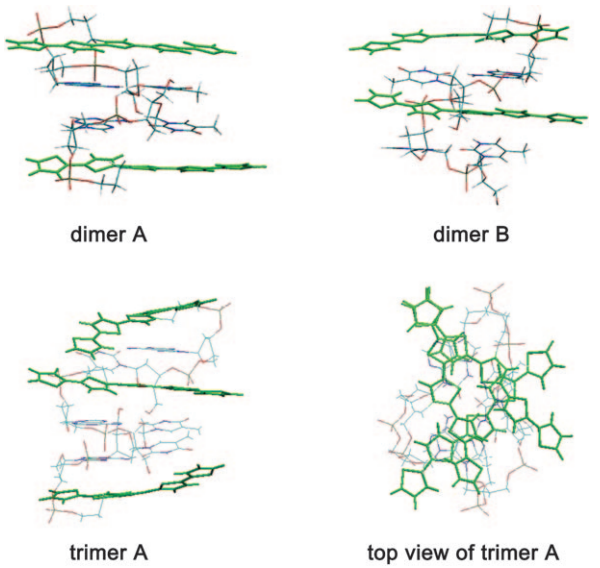

Figure 3. Most stable dimers (A and B) and most stable trimer (A) of conjugate $^{5'}$TA$^{3'}$-t5 (**8a**).

Table 1. Calculated total energies and energy components of the most stable dimers of $^{5'}$TA$^{3'}$-t5 (**8a**) and $^{5'}$CG$^{3'}$-t5 (**8b**) and of the most stable trimers of **8a**.

	ΔG [kJ mol^{-1}]	ΔE [kJ mol^{-1}]	$-T\Delta S$ [kJ mol^{-1}]
dimer A $^{5'}$TA$^{3'}$-t5	−70.92	−127.98	64.15
dimer B $^{5'}$TA$^{3'}$-t5	−66.30	−124.86	66.08
dimer C $^{5'}$TA$^{3'}$-t5	−64.33	−121.15	69.71
dimer A $^{5'}$CG$^{3'}$-t5	−68.48	−134.56	82.15
dimer B $^{5'}$CG$^{3'}$-t5	−51.83	−110.11	61.85
dimer C $^{5'}$CG$^{3'}$-t5	−94.62	−167.96	93.17
trimer A $^{5'}$TA$^{3'}$-t5	−157.80	−272.68	134.78
trimer B $^{5'}$TA$^{3'}$-t5	−143.82	−249.76	118.33

For $^{5'}$CG$^{3'}$-t5, dimer C is more stable than dimers A and B by about 27 and 43 kJ mol^{-1}, respectively (Table 1). In this case, the nucleobases form an intermolecular W&C base pair with a helical arrangement sandwiched between the two nearly planar and parallel t5 backbones (Figure 2).

For $^{5'}$TA$^{3'}$-t5, the situation is rather more complicated as the stabilization energies of different types of aggregates are very similar. Dimer A is the most stable by nearly 5 and 7 kJ mol^{-1} with respect to dimers B and C (Table 1). Figure 3 shows the arrangement of dimers A and B. In the former, the nucleobases are nearly coplanar, but do not form a W&C base pair; there are two nucleobase layers sandwiched between two nearly parallel t5 backbones; the nucleobases are at stacking distance from each other and at stacking distance from t5 (see Figure 4 in the Supporting Information). In the latter, the nucleobases again do not form a W&C base pair, but only a single nucleobase layer is stacked between two t5 backbones, while the second nucleobase layer is folded at stacking distance over a single t5.

Dimer C of **8a** (not shown) is characterized by an intermolecular W&C A···T base pair and the same arrangement as observed for bioconjugate **8b**. The lower stability of dimer C for **8a** with respect to **8b** is likely to be related to the presence of two instead of three hydrogen bonds in the base pair.

The addition of one more molecule to dimers A and B of **8a** in order to form the corresponding trimers increases the energy difference between the most stable forms. According to the data reported in Table 1, trimer A of **8a** now becomes preferred over trimer B by 14 kJ mol^{-1}. Figure 3 shows the arrangement of trimer A and the corresponding top view, indicating that the backbones of the t5 moieties are arranged in a radial way surrounded by the hydrophilic phosphate groups.

The calculations underline the importance of thiophene–nucleobase stacking interactions in the bioconjugates of quinquethiophene, as already observed for those of quaterthiophene having a different substitution pattern.[7c]

UV/Vis, photoluminescence (PL), and circular dichroism (CD) spectroscopy in solution and thin film: Conjugates **8a** and **8b** are photoluminescent compounds in water solutions and in cast films. Their UV/Vis and photoluminescence spectra in H_2O and in cast films, prepared from 10^{-3} M aqueous solutions, are shown in Figure 4, and absorption and PL wavelengths are given in Table 2.

The UV/Vis spectra in solution consist of a signal around 260 nm, attributed to the oligonucleotide moiety, and a signal around 410 nm, attributed to t5. For compounds **8a** and **8b** the PL spectrum in solution, arising from the t5 moieties, consists of a main signal split into two bands at about 500 nm, and one red-shifted shoulder in the region of 550–600 nm. These spectra are very similar to those of "free" quinquethiophene, and, in general, to those of thiophene oligomers in solution.[12]

The UV/Vis signals of both the conjugates in cast films are almost superimposable and blue-shifted by 5–9 nm with respect to those in solution, whereas the signals pertaining to the dinucleotide scaffolds remain unchanged.

PL signals in cast films are red-shifted by about 30 nm with respect to the solution. Although these blue shifts in the UV/Vis spectra and red shifts of the PL band are smaller compared to those obtained for the bioconjugates of the quaterthiophene,[7c] for compounds **8a** and **8b** the formation of H-type aggregates could also be envisaged. However, since extrinsic processes, such as exciton migration to structural defects and impurities, can influence the PL signal, more detailed studies are required before a sound interpretation of the experimental data can be given. It is worth noting that, contrary to the bioconjugates of quaterthiophene, the PL signals of **8a** and **8b** in cast films did not exhibit a remarkable sharpening with respect to the solution, suggesting that the emission signal is generated by more than one type of aggregate.

Owing to the low solubility of compound **8b** in both organic solvents and water, CD measurements were carried out only on compound **8a**.

As in the case of quaterthiophene–dinucleotide conjugates,[7c] CD measurements showed a transfer of chirality from

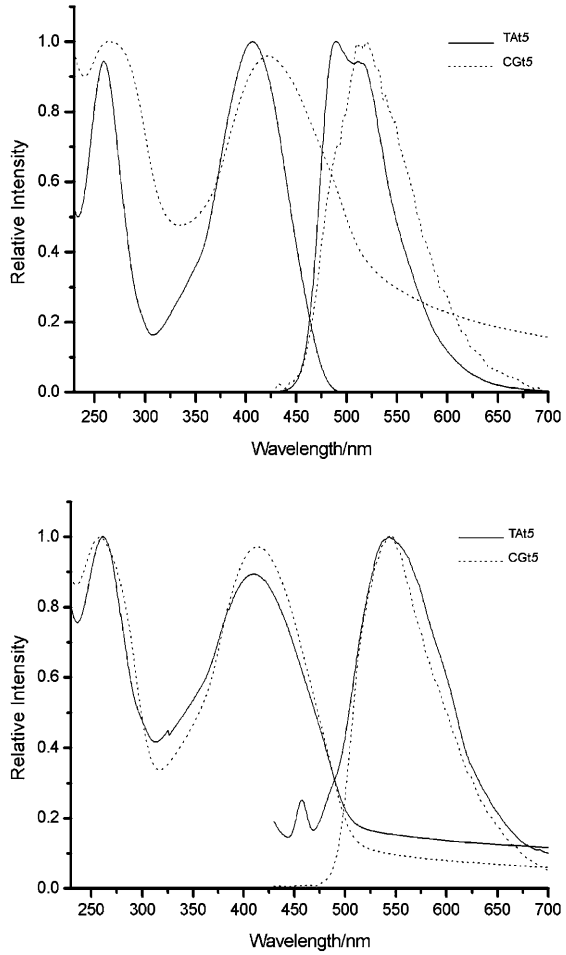

Figure 4. UV/Vis and PL spectra ($\lambda_{exc}=410$ nm) of conjugates $^{5'}$TA$^{3'}$-t5 **8a** and $^{5'}$CG$^{3'}$-t5 **8b** in aqueous solution (5.10^{-6} M) (top) and in films cast from a 5.10^{-6} M and a 10^{-3} M water solution (bottom).

Table 2. Maximum absorption and photoluminescence wavelengths of conjugates $^{5'}$TA$^{3'}$-t5 (**8a**) and $^{5'}$CG$^{3'}$-t5 (**8b**).

Compound	Conditions	λ_{max} [nm]	λ_{PL} [nm]
8a	[a]	259, 406	490, 512
	[b]	262, 411	544
8b	[a]	263, 422	520
	[b]	259, 413	547

[a] Aqueous solution, 5×10^{-6} M, pH 7.4. [b] Cast film from a 10^{-3} M solution in H_2O.

the dinucleotide substituents to the quinquethiophene moiety both in solution at high ionic strength and in cast film. The CD spectra of **8a**, 10^{-5} M in aqueous buffer (pH 7.4), in aqueous buffer containing 1 M NaCl, and in cast films from H_2O solutions are shown in Figure 5.

The corresponding CD data are reported in Table 3. The spectra consist of two regions, one with a bisignated signal at 250–280 nm assigned to the TA dinucleotide, and the other with a signal around 400 nm corresponding to the π–π* absorption region of t5 and related to long-range electronic interactions between the t5 moieties.

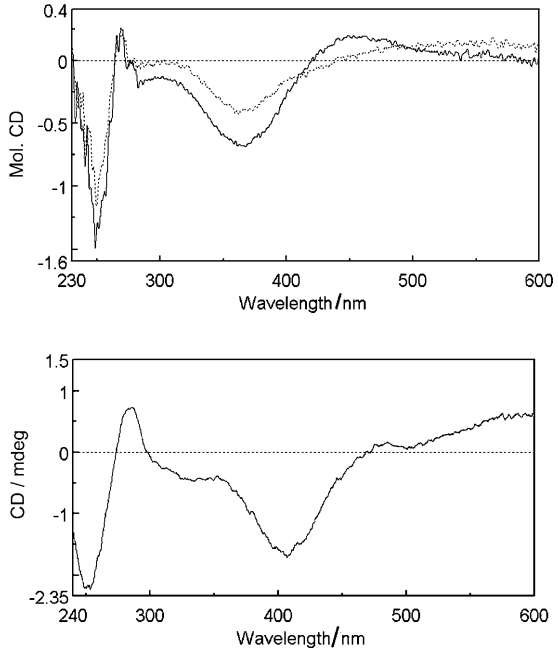

Figure 5. Circular dichroism spectra of conjugate $^{5'}$TA$^{3'}$-t5, **8a**; top: in aqueous buffer, pH 7.4 (dotted line) and aqueous buffer, pH 7.4 with 1 M NaCl (solid line); bottom: in cast film from a 10^{-3} M solution in H_2O.

Table 3. CD data for conjugate $^{5'}$TA$^{3'}$-t5 (**8a**).

Sample[a]	λ_{max} [nm]	$\Delta\varepsilon$	$g\times10^4$	ψ
1	270, 250	+0.21, −1.16	+0.08, −0.29	
	362	−0.41	−0.43	
2	269, 249	+0.26, −1.49	+0.09, −0.44	
	457, 366	+0.19, −0.68	+0.19, −0.6	
3	276, 253			+0.73, 2.23
	407			−1.71
	383			0

[a] Sample 1: Aqueous buffer, pH 7.4; sample 2: aqueous buffer, 1 M NaCl; sample 3: cast film from a 10^{-3} M solution in H_2O.

Upon increasing the ionic strength of the solution by addition of NaCl, hence on increasing molecular aggregation, the t5 signals show the appearance of a weak positive band at around 450 nm besides the signal at 362 nm already present in aqueous buffer. Note that the crossover of the apparently bisignated signal upon addition of NaCl to the solution in Figure 5a does not correspond to the maximum wavelength absorption observed both in film and in solution under the same experimental conditions.

In cast film, **8a** shows the t5 negative signal red-shifted by 55 nm (to 407 nm), with respect to that observed in solution. No exciton coupling signal was detected.

The CD spectra of **8a** present neither changes in shape nor sign inversion from solution to cast film, suggesting that the aggregates formed by this conjugate are intrinsically stable. It is worth noting that the CD data reported in Table 3 are similar to those already reported for t4 bioconjugates[7c] and for stilbene derivatives functionalized with DNA bases.[13]

The calculations offer a nice guideline for interpretation of the shape of the PL spectra of t5–dinucleotide conjugates in cast films in comparison with those of t4 conjugates. In the latter, the emitting center, t4, is encapsulated between the nucleobases; as a consequence the PL bands are very sharp in the solid state, as there is only one single type of emitting center, as if t4 were an "isolated" molecule. In the former, the emitting center, t5, is not "isolated" by the screening of the nucleobases, but surrounded by several other interacting t5 moieties. Thus, the PL bands are broad in cast film as is usually observed for unsubstituted oligothiophenes.

Microfluidic-induced self-assembly and PL and AFM characterization of bioconjugate 8a: On the basis of the calculations it is reasonable to assume that in solution different types of dimeric aggregates of **8a** are present. Consequently, we analyzed the self-organization processes of this conjugate in controlled conditions by employing microfluidic techniques.

Imbibition, filling motion, and displacement of liquids in a confined geometry are driven by capillary forces and surface effects, which dominate over the bulk dynamics.[14a,b] In particular, this means that microfluidic systems usually fulfill a fast diffusion regime, in which the interactions of liquid molecules with the surface dominate over molecular diffusion components of the capillary dynamics.[14c] Therefore, the capillarity phenomena usually result from the balance of two opposing forces: liquid adhesion to a solid surface, which tends to spread the liquid, and the cohesive surface tension force of the liquid, which acts to reduce the liquid–vapor interfacial area.[14d] Such phenomena, depending on surface effects, interfacial properties, and geometry, play a crucial role in the control of the liquid dynamics, as well as in the possibility to finely address self-assembly and supramolecular organization of functional materials in micro- and nanostructures.[14e–g] The laminar flow rate of a capillary motion is given by a power-law equation, $dz/dt \approx [(R_H)^2 \Delta p]/8\eta z$, as a function of the hydraulic radius R_H, the capillary pressure Δp, and the liquid viscosity η.[14b,h,i]

The $^{5'}TA^{3'}$-t5 (**8a**) stripes patterned by microfluidics show remarkable differences in supramolecular organization on changing the solution concentration and the kinetics of evaporation.

In particular, significant differences in the supramolecular organization have been detected for three different concentrations of **8a** in H_2O: 1) 1 mg mL^{-1}, sample A; 2) 2 mg mL^{-1}, sample B; 3) 6 mg mL^{-1} (saturated solution), sample C; 4) 6 mg mL^{-1} (saturated solution) on treated substrate, sample D. Spatially-resolved confocal investigations were performed in order to assign the PL emission to the patterned area and to the self-assembled material with nanometer resolution.

The volume of the solution, deposited and penetrated inside the microchannels by capillarity, was kept constant for all samples. In the case of samples A and B we chose to perform the fluidic experiment in laboratory atmosphere and to fix the evaporation time in order to compare the effect of solution concentration on the self-organization of **8a**. After the liquid imbibition by the channels, the elastomeric replicas were removed after about one hour. In the case of samples C and D, because of the higher viscosity of the solution, we chose to modulate the fluidic parameters by saturating the environment atmosphere during the liquid evaporation.[14b] In fact, we found that the combination of the high viscosity and the vapor saturation reduces the typical velocity of capillary motion, thus allowing better control of the molecular self-assembly inside the channels.

Atomic force microscopy (AFM) measurements of the patterned stripes of sample A (Figure 6a–c) reveal a homogeneous arrangement inside the channels with the formation of well-defined quadrangular-plate crystals, laid one on the top of the other in an orderly way. The crystals are about 1–2 μm wide and 40–100 nm high. The optical image in true color and the spatially-resolved photoluminescence, collected by a confocal microscope, show that the fluidic process has not affected the optical properties (Figure 6d and 6e).

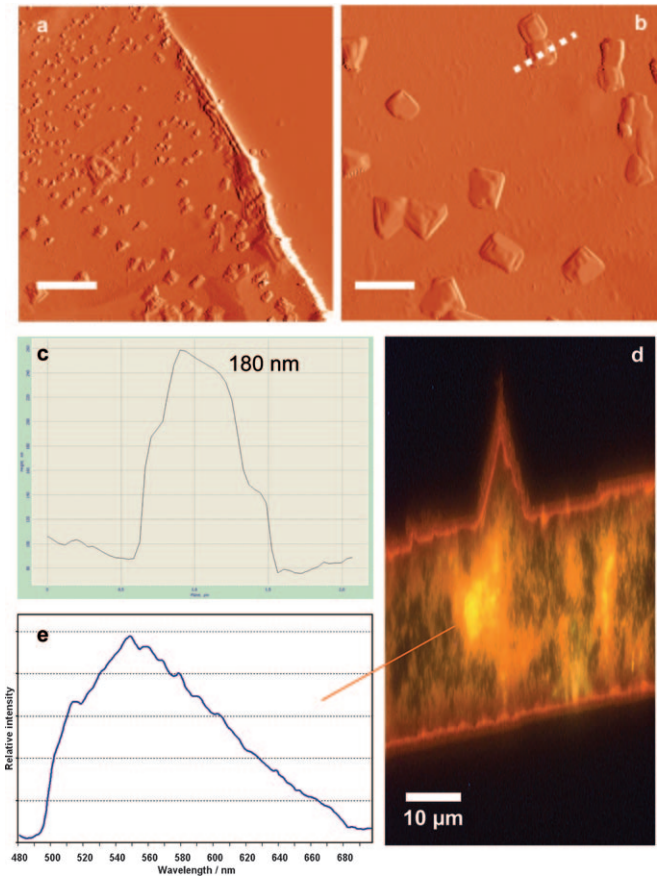

Figure 6. AFM and confocal microscopy images of quadrangular-plate aggregates in sample A, obtained using a 1 mg mL^{-1} solution of $^{5'}TA^{3'}$-t5 (**1**) in H_2O and evaporation time approximately one hour. a,b) AFM phase signal inside micro-channel (scale bar in a) 5 μm, in b) 2μm); c) vertical section of quadrangular-plate crystals; d) optical image in true colours; e) PL spectra collected by spatially resolved confocal microscopy.

The PL spectrum, in Figure 6e, with a maximum at 540–550 nm, is similar to that of t5 in solution and in cast film.

The morphology of the patterned layer in sample B (Figure 7) shows that conjugate **8a** self-organizes under capillary driving forces in a supramolecular spherulitic structure made up of rodlike crystals, spatially arranged at precise angles. Spherulite morphology is commonly observed in block copolymers that have hydrophilic and hydrophobic blocks. Here, the different molecular concentration seems to affect the supramolecular structure by inducing a self-assembly driven by a sort of nucleation centre.[14l,m] Moreover, there is no relevant difference in the optical properties (Figure 7a and 7b). A deeper investigation of sample B by AFM reveals macroscopic features with a lateral dimension of about 10 μm and an average thickness of nanometric dimensions (10–20 nm). The rodlike crystals, which are the basic units of the spherulitic structure, have a width of about 500 nm, while the spherical nucleation centre is about 1 μm or more wide (Figure 7c–f).

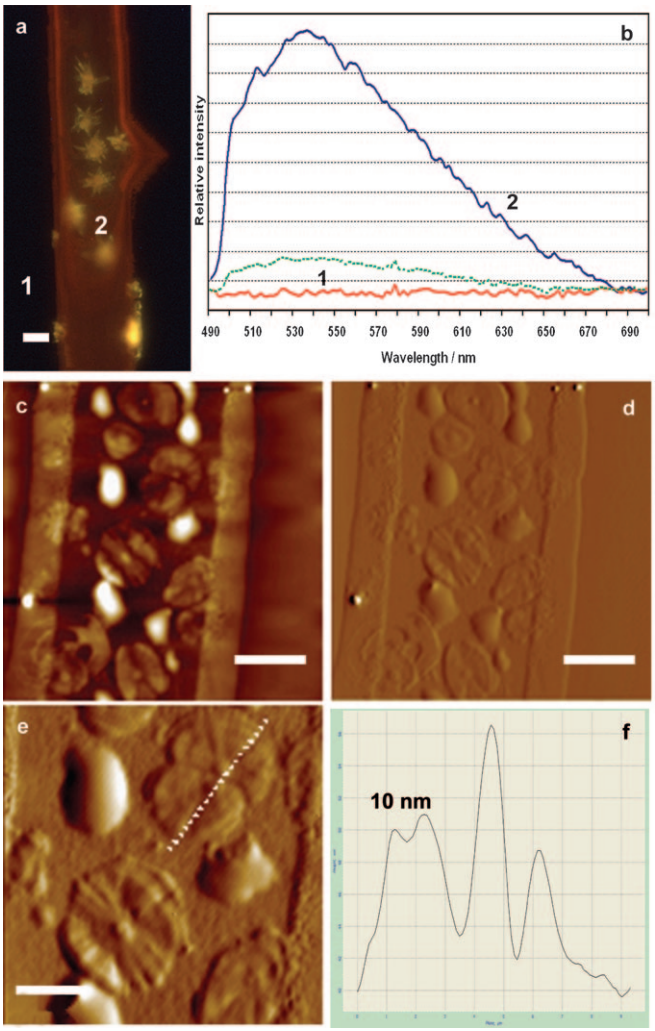

Figure 7. AFM and confocal microscopy images of spherulitic aggregates in sample B, obtained using a 2 mg mL^{-1} solution of ^{5}TA^{3}-t5 (**1**) in H_2O and evaporation time approximately one hour. a) Optical image in true colours (scale bar 10 μm); b) PL spectra collected by spatially resolved confocal microscopy outside (1) and inside (2) the channel (the green trace corresponds to another region inside the channel); c,d) AFM topography and phase signal inside micro-channel (region 2; scale bars 10 μm)); e,f) AFM phase signal of self-assembled structures (scale bar 5 μm) and the vertical section profile of a spherulitic aggregate.

In samples C and D, owing to the increase in solution concentration and the consequent reduction of the capillary velocity, the evaporation time of water increased and a fine control of the driving flow was achieved. More importantly, the reduction of the fluid velocity and the saturation of the external conditions during the dynamical process matched up, thus realizing a better control of the self-assembly process and enhancing the order in the supramolecular organization of conjugate **8a**.

The optical image of sample C (Figure 6 in the Supporting Information) shows a homogeneous arrangement inside the micro-channel. A deeper investigation by AFM reveals macroscopic supramolecular structures, arranged in a sort of radial way on different scales, surrounded by amorphous material (Figure 6a–e in the Supporting Information). In fact, it is possible to see, in the middle section of the channels, the formation of spherulitic structures similar to those observed in sample B, made up of rodlike crystals arranged around a nucleation centre in a radial way (Figure 6c, d in the Supporting Information). In contrast, the outside of the supramolecular structure, at the end of the capillary front flow (Figure 6a in the Supporting Information) and near the edges of the micro-channels (Figure 6b in the Supporting Information), shows the beginning of a dendrimeric supramolecular structure with a height of about 1 μm, 10–20 μm long and 2–3 μm wide.

To favor the formation of supramolecular structures over the channel width, we treated the substrate with a mild oxygen plasma, to improve the hydrophilic interactions of the aqueous solution inside the capillary. Figure 8 shows the AFM topography of the striped pattern in sample D and the formation of a dendrimeric supramolecular structure. We can recognize in the morphology of **8a** the same rodlike crystals arranged at precise angles around a vertical axis, which acts as a nucleation site. The images in Figure 8 reveal that the self-assembly process leads to a supramolecular structure that takes up all the available channel area. Moreover, Figure 8e and f show that the aggregate emission, with a maximum at about 530 nm detected by confocal spatially-resolved PL spectra, is blue-shifted compared to that of the other samples displaying a maximum around 540 nm.

These results confirm that the surface effects, prevalent in a microfluidic process, act on the self-assembly of conjugate **8a** by enhancing the main intermolecular interactions in the flow direction with the formation of different types of aggregates. Anyway, the fluorescence emission of the microfluidic patterned film are similar to those from cast film, thus confirming that the effects of elastic stress, due to the internal capillary pressure, on the conjugate **8a** are almost negligible.

It is worth noting that the concentration range in which the morphology changes observed take place is rather small, indicating the presence of several types of intermolecular

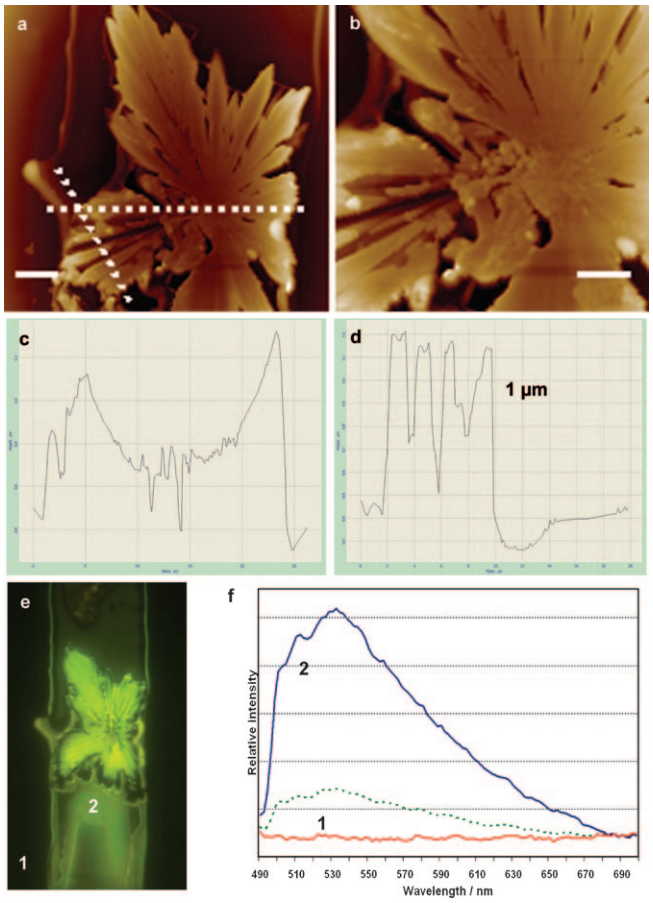

Figure 8. AFM and confocal microscopy images of dendrimeric aggregates in sample D, obtained using a saturated solution of $^{5'}$TA$^{3'}$-t5 (**1**) in H_2O on treated substrate and evaporation time modulated during the driving motion, in order to reduce the typical velocity of a capillary. a,b) AFM topography of a self-assembled structure inside microchannel (scale bar in a) 5 μm; in b) 2 μm); c,d) section profiles of two different parts of the dendrimeric aggregate; e) optical image in true colours; f) PL spectra collected by spatially resolved confocal microscope outside (1) and inside (2) the channel (the green trace corresponds to another region inside the channel); c,d) AFM topography and phase signal inside micro-channel (region 2).

forces contributing in a synergic way to the formation of the aggregates.

Electrical characterization of bioconjugate 8a: The transport properties of cast films of conjugate **8a** were investigated using the same two-electrode device already described in the case of oligonucleotide–t4 conjugates.[7c] The device substrate consisted of two interdigitated Au electrodes, fabricated by evaporating gold onto oxidized silicon wafers and patterned with photolithography (Figure 7 of the Supporting Information) onto a ceramic support. Given the structure of the two interdigitated electrodes, the distance between adjacent fingers, 20 μm, was the conductor length (L). The area of the conductor was calculated from the cross-section of the volume between two adjacent fingers (channel), given by the product of the finger length and the finger height (the thickness of the gold metal). The area of a single channel was multiplied by the number of channels in order to obtain the total area of the conductor.

Solution-cast films of **8a** in H_2O were deposited onto the substrates with a concentration (0.25 mg mL^{-1}) comparable to that resulting in the formation of lamellar aggregates in microfluidic-induced self-assembly experiments. To avoid ionic conduction activated by moisture,[7c] the electrical characterization was performed under a dynamic vacuum of 2×10^{-5} mbar and the samples were left in the measurement chamber for several hours under dynamic vacuum, until a constant current was observed with time under constant d.c. applied voltage, before starting the electrical characterization; then system hole conductivity can be measured.[7c]

Figure 9 shows the current density versus voltage (J–V) characteristics of a film of **8a** on interdigitated Au electrodes. It obeys Ohm's law at low voltages, where the current shows a good quadratic dependence on the voltage.

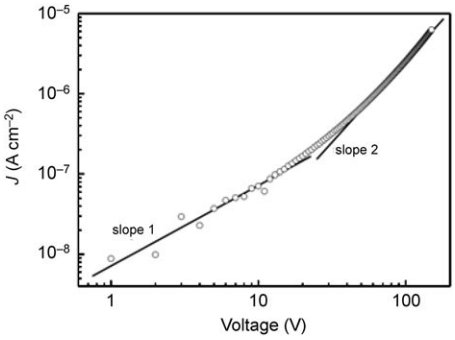

Figure 9. Log–log plot of the J–V characteristic of a film of $^{5'}$TA$^{3'}$-t5 (**8a**) on gold interdigitated electrodes. The measurement was carried out at room temperature and under dynamic vacuum of 2×10^{-5} mbar.

This behavior is typical of space-charge limited current (SCLC),[15a] given by $j=9/8\,\varepsilon_0\varepsilon_r\mu V^2L^{-3}$ in the trap-free regime, in which ε_0 is the vacuum permittivity, ε_r is the relative dielectric constant of the material, μ is the charge carrier mobility and L is the electrode separation. Even when the trap-free limit is not experimentally accessible, the above formula can be used to extract a lower limit for the intrinsic mobility of the material, at least in the case in which one type of carrier (holes in the present case) is responsible for charge transport. By using $\varepsilon_r=3$, a hole mobility of 5.8×10^{-6} cm^2 V^{-1} s^{-1} was calculated for **8a**. This mobility value has to be considered as a lower limit for the hole mobility of **8a**, the SCLC current being reduced by the presence of traps. This mobility is about four orders of magnitude lower than that measured for unsubstituted α-quinquethiophene in vacuum-evaporated thin films.[10b] However, it is 1–2 orders of magnitude larger than that measured for t4–dinucleotide conjugates,[7c] probably due to both the larger oligomer size and the greater proximity between the t5 moieties.

Conclusion

Our data point to the fact that the self-organization modalities of oligothiophene–dinucleotide conjugates cannot be explained only on the basis of hydrogen-bondings between complementary nucleobases. Clearly, in bioconjugates one cannot take into account only one part of the molecule and assume that its interactions are the same as when this part is not linked to another entity. New types of interactions may indeed be generated, which may lead to unpredicted aggregation modalities.

This is the case for $^{5'}$TA$^{3'}$-t5 (**8a**), in which the growth is not directed by intermolecular W&C hydrogen bonds between the A···T moieties of interacting molecules, but is instead governed by intra- and intermolecular thiophene–nucleobase stacking interactions. Significantly, these interactions were demonstrated to govern also the growth of the bioconjugates of quaterthiophene with TA, AA, and TT dinucleotides, in which the size of the semiconductor moiety was smaller and the substitution pattern different from the bioconjugates of quinquethiophene described here.[7c]

On the other hand, the theoretical calculations on $^{5'}$CG$^{3'}$-t5 (**8b**) indicate that when the nucleobases can form more stable hydrogen-bonded W&C base pairs, both canonical hydrogen bondings and thiophene–nucleobase stacking interactions might contribute to the formation of helical aggregates. Unfortunately, in the case of **8b**, the aggregates are so stable that they are almost insoluble. One should then study some kind of functionalization of the thienyl rings with groups capable of increasing the solubility without subverting the main interactions.

In both the t5–dinucleotide aggregates discussed here and the already reported t4–dinucleotide aggregates,[7c] thiophene backbones are screened by the nucleobases and separated from each other by a distance much greater than that observed for stacked unsubstituted quinque- and quaterthiophenes.[17] So, it is not surprising that the estimated hole mobility of the conjugates is a few orders of magnitude lower than that measured for unsubstituted t4 and t5 in evaporated films. Indeed, charge carrier mobility is strictly related to semiconductor–semiconductor orbital overlap.[4,10]

While the screening of the semiconductor components by the nucleobases disfavors charge transport in the aggregates, the separation between oligothiophene components realized in this way favors photoluminescence. It is known that close proximity of the aromatic backbones leads to PL quenching in aggregates of unsubstituted thiophene oligomers.[18] In contrast, owing to the great distance between adjacent t4 or t5 moieties, intense photoluminescence emission could be observed for the aggregates of t4 and t5 bioconjugates.

In conclusion, the films of oligothiophene–oligonucleotide conjugates are electroactive, photoluminescent, and even chiral, owing to chirality transfer from the dinucleotides to the oligothiophenes. Enhancing one or the other of these properties will depend on the appropriate choice of oligomer size, type of biocomponent, and substitution pattern, which will determine the balance of interactions guiding molecular recognition.

Experimental Section

Microfluidic lithography: Microfluidic networks were obtained by structured elastomeric elements in poly(dimethylsiloxane) (PDMS) in conformal contact with a silicon substrate. PDMS moulds were realized by replica molding from silicon masters, with a microchannel network of about 28 μm-wide parallel stripes, spaced at about 98 μm, and a depth of 1.7 μm.[12a,b] The silicon Si(1,0,0) substrates were cleaned before use in an ultrasonic bath with acetone and isopropylalcohol. In order to achieve better hydrophilic surface properties, favoring the capillary penetration of water solutions inside microchannels, we performed an O_2 plasma treatment on Si substrates ($t = 3$ s, rf power = 50 W, pressure = 52 mTorr). The replicas were imbibed with aqueous solutions of $^{5'}$TA$^{3'}$-t5 (**8a**) at different concentrations, which filled the elastomeric channels by the capillary effect. After the complete evaporation of water, the PDMS moulds were peeled off, leaving a striped pattern of molecular material deposited on the silicon substrate.

Atomic force microscopy: AFM images were taken using a Solver Pro, NT-MDT instrument working in semicontact mode.

Optical microscopy: The optical images and the photoluminescence (PL) spectra were taken using a confocal laser scanning microscope FluoView 1000, Olympus, with an *xy* resolution of about 200 μm.

UV/Vis and CD spectroscopy: Absorption spectra were taken on a Perkin–Elmer Lambda 20 spectrometer, and CD spectra were recorded by using a spectropolarimeter JASCO J-715 under ambient conditions.

Electrical characterization: Substrates consisted of two interdigitated comb-like gold electrodes deposited onto a layer of silicon dioxide thermally grown on silicon plates. Each electrode was composed of 13 fingers 4 mm long. The thickness of the oxide was 1 μm and that of the metal layer was 0.6 μm. The distance between two consecutive gold fingers (the spacing between the two electrodes) was 20 μm. The active area, calculated from the free space between the gold fingers, was 4.35×10^{-4} cm^2. Films of **8a** were deposited onto the substrates by casting an aqueous solution (5 μL) in order to completely cover the interdigitated area. The concentration of the solution was 25 g L^{-1}, leading to films with a thickness higher than that of the electrode layer. The film thickness, measured with a Tencor Alphastep 200 profilometer, was in the range 1.1–1.4 μm. The samples were dried under ambient conditions. The electrical characterization was performed, at ambient temperature, under dynamic vacuum (2×10^{-5} mbar). The current–voltage curves were taken by using a Keithley 487 source-picoammeter.

Acknowledgement

This work was partially funded by the FIRB RBNE03S7XZ 005 (SYNERGY) project. I.V. thanks S. D'Amone for technical support.

[1] a) A. N. Sokolov, D. C. Swenson, L. R. MacGillivray, *Proc. Natl. Acad. Sci. USA* **2008**, *105*, 1794–1797; b) O. J. Dautel, M. Robitzer, J. C. Flores, D. Tondelier, F. Serein-Spirau, J. P. Lère-Porte, D. Guérin, S. Lenfant, M. Tillard, D. Vuillaume, J. J. E. Moreau, *Chem. Eur. J.* **2008**, *14*, 4201–4213; c) G. Barbarella, M. Zambianchi, A. Bongini, L. Antolini, *Adv. Mater.* **1993**, *5*, 834–838; d) E. A. Marseglia, F. Grepioni, E. Tedesco, D. Braga, *Mol. Cryst. Liq. Cryst.* **2000**, *348*, 137–151.

[2] a) Y. Ie, Y. Umemoto, M. Okabe, T. Kusunoki, K. Nakayama, Y. J. Pu, J. Kido, H. Tada, Y. Aso, *Org. Lett.* **2008**, *10*, 833–836; b) A. R. Murphy, J. M. Fréchet, *Chem. Rev.* **2007**, *107*, 1066–1096; c) M. H. Yoon, A. Facchetti, C. E. Stern, T. J. Marks, *J. Am. Chem. Soc.* **2006**,

128, 5792–5801; d) H. Sirringhaus, *Adv. Mater.* **2005**, *17*, 2411; e) G. Barbarella, M. Melucci, G. Sotgiu, *Adv. Mater.* **2005**, *17*, 1581–1593.

[3] a) T. Siegrist, R. M. Fleming, R. C. Haddon, R. A. Laudise, A. J. Lovinger, H. E. Katz, P. Bridenbaugh, D. D. Davis, *J. Mater. Res.* **1995**, *10*, 2170–2173; b) T. Siegrist, C. Kloc, R. A. Laudise, H. E. Katz, R. C. Haddon, *Adv. Mater.* **1998**, *10*, 379–382; c) G. Barbarella, M. Zambianchi, L. Antolini, P. Ostoja, P. Maccagnani, A. Bongini, E. A. Marseglia, E. Tedesco, G. Gigli, R. Cingolani, *J. Am. Chem. Soc.* **1999**, *121*, 8920–8926; d) H. Muguruma, T. K. Saito, S. Hotta, *Thin Solid Films* **2003**, *445*, 26–31.

[4] a) C. D. Dimitrakopoulos, P. R. L. Malenfant, *Adv. Mater.* **2002**, *14*, 99–117; b) A. R. Murphy, J. M. J. Fréchet, *Chem. Rev.* **2007**, *107*, 1066–1096; c) A. Facchetti, *Mater. Today* **2007**, *10*, 28–37; d) L. L. Chua, J. Zaumseil, J. F. Chang, E. C. W. Ou, P. K. H. Ho, H. Sirringhaus, R. H. Friend, *Nature* **2005**, *434*, 194–199.

[5] a) P. Leclère, M. Surin, P. Viville, R. Lazzaroni, A. F. M. Kilbinger, O. Henze, W. J. Feast, M. Cavallini, F. Biscarini, A. P. H. J. Schenning, E. W. Meijer, *Chem. Mater.* **2004**, *16*, 4452–4466; b) S. Westenhoff, A. Abrusci, W. J. Feast, O. Henze, A. F. M. Kilbinger, A. P. H. J. Schenning, C. Silva, *Adv. Mater.* **2006**, *18*, 1281–1285.

[6] F. E. Alemdaroglu, A. Herrmann, *Org. Biomol. Chem.* **2007**, *5*, 1311–1320.

[7] a) R. Iwaura, F. J. M. Hoeben, M. Masuda, A. P. H. J. Schenning, E. W. Meijer, T. Shimizu, *J. Am. Chem. Soc.* **2006**, *128*, 13298–13304; b) A. Jatsch, A. Kopyshev, E. Mena-Osteritz, P. Baüerle, *Org. Lett.* **2008**, *10*, 961–964; c) S. Alesi, G. Brancolini, M. Melucci, M. Luigi Capobianco, A. Venturini, N. Camaioni, G. Barbarella, *Chem. Eur. J.* **2008**, *14*, 513–521; d) N. L. Rosi, C. A. Mirkin, *Chem. Rev.* **2005**, *105*, 1547–1562; e) G. P. Spada, S. Lena, S. Masiero, S. Pieraccini, M. Surin, P. Samori, *Adv. Mater.* **2008**, *20*, 2433–2438.

[8] a) H. A. Ho, M. Boissinot, M. G. Bergeron, G. Corbeil, K. Doré, D. Boudreau, M. Leclerc, *Angew. Chem.* **2002**, *114*, 1618; *Angew. Chem. Int. Ed.* **2002**, *41*, 1548–1551; b) B. S. Gaylord, A. J. Heeger, G. C. Bazan, *Proc. Natl. Acad. Sci. USA* **2002**, *99*, 10954–10957; c) K. P. R. Nilsson, O. Inganäs, *Nat. Mater.* **2003**, *2*, 419–424; d) S. W. Thomas III, G. D. Joly, T. M. Swager, *Chem. Rev.* **2007**, *107*, 1339–1386.

[9] a) F. Garnier, R. Hajlaoui, A. El Kassmi, G. Horowitz, L. Laigre, W. Porzio, M. Armanini, F. Provasoli, *Chem. Mater.* **1998**, *10*, 3334–3339; b) X. Cai, C. P. Gerlach, C. D. Frisbie, *J. Phys. Chem. C* **2007**, *111*, 452–456; c) M. H. Yoon, S. A. DiBenedetto, M. T. Russel, A. Facchetti, T. J. Marks, *Chem. Mater.* **2007**, *19*, 4864–4881.

[10] a) A. R. Murphy, J. M. Fréchet, *Chem. Rev.* **2007**, *107*, 1066–1096.

[11] a) J. Scott, P. A. Weiner, D. A. Kollman, U. Case, *J. Comput. Chem.* **1990**, *11*, 440–467; b) C. Singh, C. Ghio, G. Alagona, S. Profeta, P. Weiner, *J. Am. Chem. Soc.* **1984**, *106*, 765–784; c) S. Chowdhury, M. Bansal, *J. Biosci.* **2001**, *26*, 649–665; d) W. C. Still, A. Tempczyk, R. C. Hawley, T. Hendrickson, *J. Am. Chem. Soc.* **1990**, *112*, 6127–6129.

[12] a) Y. Kanemitsu, K. Suzuki, Y. Masumoto, *Phys. Rev. B* **1994**, *50*, 2301–2305; b) R. S. Becker, J. Seixas de Melo, A. L. MaÅanita, F. Elisei, *J. Phys. Chem.* **1996**, *100*, 18683–18695.

[13] F. D. Lewis, Y. Wu, L. Zhang, X. Zuo, R. T. Hayes, M. R. Wasielewski, *J. Am. Chem. Soc.* **2004**, *126*, 8206–8215.

[14] a) Y. Xia, G. M. Whitesides, *Angew. Chem.* **1998**, *110*, 568; *Angew. Chem. Int. Ed.* **1998**, *37*, 550; b) I. Viola, D. Pisignano, R. Cingolani, G. Gigli, *Anal. Chem.* **2005**, *77*, 591–595; c) R. Kimmich, *Chem. Phys.* **2002**, *284*, 253–285; d) D. Myers, *Surface, Interface, and Colloids: Principles and Applications*, Wiley-VCH, Weinheim, **1999**; e) I. Viola, M. Mazzeo, A. Passabi, S. D'Amone, R. Cingolani, G. Gigli, *Adv. Mater.* **2005**, *17*, 2935–2939; f) I. Viola, F. Della Sala, M. Piacenza, L. Favaretto, M. Gazzano, G. Barbarella, R. Cingolani, G. Gigli, *Adv. Mater.* **2007**, *19*, 1597–1602; g) J. N. Israelachvili, *Intermolecular and Surface Forces*, Academic Press, London, **1992**; h) E. Delamarche, A. Bernard, H. Schmid, B. Michel, H. Schmid, A. Bietsch, B. Michel, H. Biebuyck, *J. Am. Chem. Soc.* **1998**, *120*, 500–508; i) R. D. Deegan, O. Bakajin, T. F. Dupont, G. Huber, S. R. Nagel, T. A. Witten, *Nature* **1997**, *389*, 827–829; j) U. Thiele, M. Mertig, W. Pompe, *Phys. Rev. Lett.* **1998**, *80*, 2869–2872.

[15] a) M. A. Lampert, P. Mark, *Current Injection in Solids*, Academic Press, New York, **1970**; b) V. Coropceanu, J. Cornil, D. A. da Silva Filho, Y. Olivier, R. Silbey, J. L. Brédas, *Chem. Rev.* **2007**, *107*, 926–952.

[16] M. Melucci, M. Gazzano, G. Barbarella, M. Cavallini, F. Biscarini, P. Maccagnani, P. Ostoja, *J. Am. Chem. Soc.* **2003**, *125*, 10266–10274.

[17] O. Henze, W. J. Feast, F. Gardebien, P. Jonkheijm, R. Lazzaroni, P. Leclère, E. W. Meijer, A. P. H. J. Schenning, *J. Am. Chem. Soc.* **2006**, *128*, 5923–5929.

[18] a) D. Oelkrug, H. J. Egelhaaf, J. Gierschner, A. Tompert, *Synth. Met.* **1996**, *76*, 249–253; b) Y. Kanemitsu, N. Shimizu, K. Suzuki, Y. Shiraishi, M. Kuroda, *Phys. Rev. B* **1996**, *54*, 2198–2204.

Received: August 14, 2008
Published online: January 8, 2009

